



Reza Saremian · Majid Jamal-Omidi · Jamasb Pirkandi

# Numerical investigation on auxetic angle-ply CFRP composite laminates under low-velocity impact loading

Received: 4 February 2024 / Accepted: 28 August 2024

© The Author(s), under exclusive licence to Springer-Verlag GmbH Germany, part of Springer Nature 2024

**Abstract** Materials with a negative Poisson's ratio are known as auxetic materials, which are highly desirable for improved resistance to indentation and impact. Angle-ply composite laminates with high anisotropy exhibit auxetic behavior within a specific range of layup angles. In this research, the influence of negative Poisson's ratio on the mechanical response and the enhancement of the damage behavior of carbon/epoxy composite laminates under low-velocity impact has been numerically investigated. For this purpose, a MATLAB code based on classical lamination theory relationships was developed to determine the range of layup angles to achieve both negative Poisson's ratio in-plane and through-thickness (out-of-plane). Then, the layups with the most negative through-thickness and in-plane Poisson's ratio values were selected. Also, two new stacking sequences were investigated so that both of them partially exhibited the characteristic of negative through-thickness and in-plane Poisson's ratio. The progressive damage model is written and implemented using a computer code in the Abaqus user-material subroutine. The progressive damage model consists of Hashin and Puck failure criteria and the damage evolution model based on the equivalent strain method to predict the initiation and evolution of damage for matrix and fiber. The results indicate that the new laminate configurations have 66% higher effective longitudinal modulus and 173% higher effective transverse modulus compared to the in-plane and through-thickness auxetic ones, respectively. In addition, the proposed configurations showed less overall damage under low-velocity impact loading compared to the auxetic laminates. Based on the investigations, the new configurations with features such as high impact force, low impact time, and low maximum displacement could be suitable for use in structures with a hardwall design approach.

**Keywords** Auxetic composite laminates · Negative Poisson's ratio · Low-velocity impact · Numerical modeling · Finite element analysis · Hardwall

## 1 Introduction

Composites are among the most promising and prominent materials available in the current century. Currently, there is a growing demand in the industry for lightweight materials with high strength that are suitable for specific applications. Hence, composites reinforced with synthetic or natural fiber have become increasingly important. The outstanding performance of fiber-reinforced composites in numerous applications has positioned them as a promising substitute for metals and alloys [1–3]. In contrast to metal and ceramic matrix composites, polymer matrix composites (PMCs) are the most common [4]. Carbon fiber-reinforced polymer (CFRP) matrix composites are increasingly being used in industries such as automotive, energy, aerospace, marine, civil, and sport due to their superior properties, such as high specific strength and specific stiffness,

R. Saremian · M. Jamal-Omidi (✉) · J. Pirkandi  
Faculty of Aerospace Engineering, Malek-Ashtar University of Technology, Tehran, Iran  
e-mail: j\_omidi@mut.ac.ir; m.jamalomid@gmail.com

excellent corrosion resistance and fatigue, and low thermal expansion coefficient [5–7]. However, these materials have major drawbacks, including being fragile and particularly sensitive to impact. This level of impact sensitivity leads to over-sized dimensions, thus reducing their ability to ensure residual strength after impact, as well as complicating the repair of impact damage [8].

Most of the common materials become thick (thin) under compression (tension), and therefore, exhibit a positive Poisson's ratio behavior. On the other hand, materials with a negative Poisson's ratio (auxetic) exhibit contradictory behavior under axial loading. These materials become thin (thick) under compression (tension). Auxetic materials exhibit a unique type of deformation characteristic under the effect of indentation; so, the materials around the load application area tend to concentrate toward the point of force effect (impact), which causes a significant increase in local hardness. Meanwhile, under similar loading conditions, materials with a positive Poisson's ratio expand outward and make indentation easier [9]. Today, auxetic materials have become very attractive to the scientific community due to their appealing properties such as increased strength, better acoustic behavior, improved fracture toughness, excellent energy absorption, enhanced damping, and indentation resistance. So far, various types of auxetic materials and structures have been discovered and created in both micro and large sizes [10–12]. Such materials or structures are uncommon in nature and therefore are often artificially engineered. There are various methods for engineering auxetic structures. The most common approach involves using porous structures, such as chiral [13] or re-entrant [14] structures. Another approach involves the use non-porous angle-ply composite laminates, which can be designed to create a negative Poisson's ratio at effective owing to the strain mismatch between adjacent layers and the large anisotropy of the individual ply. Therefore, one potential approach to improve the low-velocity impact damage tolerance of CFRP composites is to create effective negative Poisson's ratios [15], which can be achieved by tailoring the layout of an anisotropic composite laminate [5].

Various studies have been conducted to investigate the behavior and mechanical properties of composite structures with a porous or auxetic lattice core in impact loading. Among them, Jiang et al. [16] assessed a three-dimensional finite element model (FEM) to simulate the mechanical behavior of auxetic composites under low-velocity impact loading. They used three different impact velocities of 1.50, 2.05, and 2.67 m/s to simulate the impact process of auxetic composites. Hou et al. [17], on the other hand, conducted a comparative study on the reliability of auxetic and non-auxetic lattice structures. The sample under investigation consisted of two unidirectional (UD) composite plates made of CFRP and a 3D-printed polymer core. Low-velocity impact tests were then performed to determine the deformation pattern of the unit cell and its effect on the behavior of the core structure, as well as the performance of the sandwich panel. The results indicate that the auxetic re-entrant core demonstrated superior performance in reducing power and energy loss. Furthermore, Novak et al. [18] conducted experimental and numerical investigations on the quasi-static and ballistic performance of a composite panel with a chiral auxetic lattice core made of titanium alloy. Also, tensile and ballistic loading tests were conducted on the cover plates to assess their behavior under quasi-static, dynamic, and high strain rate. The results showed that the ballistic performance of the sandwich panel with an auxetic core was increased compared to the cover ones. Usta et al. [19] also experimentally and numerically studied the behavior of composite sandwich panels with different types of auxetic and non-auxetic lattice cores in low-velocity impact loading. The results indicated that auxetic cores provided more impact resistance and energy absorption compared to their non-auxetic counterparts. Also, Xue et al. [12] conducted experimental and numerical research on the compressive properties of three component auxetic structures, which included an auxetic lattice structure, polymer filler, and steel tube. The study results indicated that the three-component structures, which included the tube, lattice structure, and polymer filler material, demonstrated superior compressive and energy absorption properties compared to both the empty tube and the lattice structure filled with polymer. Tomita et al. [20] conducted experimental and numerical research on head protection in a vehicle crash situation, based on the transition of the deformation mode from bending to auxetic compression. The results indicated that the transition of deformation modes within auxetic structures was advantageous for efficiently protecting the human body. Petit et al. [21] studied the compressive response of re-entrant auxetic structures under impact loads. They conducted an analytical model for the successive collapse of the cells. Simulations were conducted to examine the compressive response at a constant velocity or under an initial impact velocity. The results demonstrated the impact reduction capacity of the auxetic structure. The impact response of the sandwich panel with the auxetic core under low-velocity impact using high-order shear and normal deformation theory (HSNDT) was investigated by Biglari et al. [22]. In terms of minimizing deflection, the results indicate that the auxetic honeycomb sandwich panel outperforms the non-auxetic honeycomb panel by 25%. In addition, some research has focused on improving the impact resistance of composite laminates through the usage of nanocomposites [23–25].

Most of the research on the impact resistance of auxetic composite structures has focused on studying porous or lattice structures. Meanwhile, one way to increase the impact resistance of composites is by tailoring angle-ply composite laminates in an auxetic manner, a concept that has been less explored. In this regard, Alderson et al. [26] experimentally investigated and compared the low-velocity impact resistance of CFRP composite laminates with a close to zero and positive Poisson's ratio. Their results showed that at low levels of impact energy, the impact resistance of auxetic laminates was better, which indicated that there could be rate dependence in the response of auxetic laminates. Wang [15] also numerically studied the effect of the negative through-thickness Poisson's ratio on the low-velocity impact behavior of CFRP composite laminates. The finite element analysis (FEA) results indicated that the tensile damage of the fiber and the matrix in the auxetic laminates was reduced by 40%, on average, as compared to their non-auxetic counterparts. However, the auxetic laminates do not have an obvious advantage in reducing the delamination damage or the matrix compressive damage. Further, Lin et al. [5] numerically investigated the effect of negative in-plane Poisson's ratio on the low-velocity impact behavior of CFRP composite laminates. To compare the mechanical properties, they also analyzed composite laminates with a positive Poisson's ratio. The results indicated that the delamination areas in the top and bottom interfaces and matrix compressive damaged areas in the top and bottom plies of the in-plane auxetic laminates at the impact energies of 5 and 8 J were, on average, decreased by 12.6% and 38%, respectively. Also, for the impact energy of 5 J, the matrix tensile damage of in-plane auxetic laminates was reduced in the two upper plies and the two lower ones. In addition, the tensile damage of the in-plane auxetic laminate fiber showed an average reduction of 14.6%.

Considering the high costs of experimental tests and also, the difficulty of recording progressive damage behavior during impact loading tests, many researchers have preferred numerical methods to study the behavior and response of composites under impact loading conditions. However, there have been quantitative studies conducted on the low-velocity impact resistance of auxetic CFRP composite laminates so far. Meanwhile, the problem of the damage behavior of auxetic CFRP composite laminates remains largely unknown. Thus, achieving a proper understanding of the damage behavior of auxetic CFRP composite laminates will lead to improved performance and their use in impact-resistant structural applications. Since it is not possible to achieve an angle-ply composite laminate with negative in-plane and through-thickness Poisson's ratio at the same time [27]. Also, previous research demonstrated that in-plane [5] and through-thickness [15] auxetic laminates were not superior to their non-auxetic counterparts in all damage modes. Therefore, innovative designs aiming to simultaneously achieve the positive properties of both in-plane and through-thickness auxetic behaviors are of interest. In this study, a MATLAB code based on classical lamination theory (CLT) relationships [28, 29] was used to implement angle-ply CFRP composite laminates with in-plane and through-thickness auxetic behaviors. Additionally, new configurations of angle-ply CFRP composite laminates were developed to exploit both in-plane and through-thickness auxetic behaviors simultaneously. These new configurations generally exhibit non-auxetic behavior, but their partial behavior includes both in-plane and through-thickness auxetic behavior. Numerical simulations were carried out using the finite element method and the dynamic/explicit solver of ABAQUS software to examine the influence of negative Poisson's ratio on the low-velocity impact response of angle-ply CFRP composite laminates. The study was conducted on the angle-ply CFRP composite laminates with a geometry size of  $150 \times 100 \times 4$  mm. To improve calculation efficiency and simplify the model, adjacent plies with the same orientation were treated as a single ply. Consequently, the final model consisted of eight layers, with each ply being 0.5 mm thick. The user-defined material subroutine (VUMAT) was implemented to model progressive damage of angle-ply CFRP composite laminates. The mechanical response and damage behavior of in-plane and through-thickness auxetic composite laminates, as well as new configurations introduced at 25 J impact energy, were compared.

## 2 Negative in-plane Poisson's ratio, $\nu_{21}$ , laminates

According to the CLT [28], the off-axis stress–strain relationship is offered in Eq. (1) in terms of compliance. The subscript 6 is used to determine the shear component,

$$\begin{bmatrix} \varepsilon_1 \\ \varepsilon_2 \\ \varepsilon_6 \end{bmatrix} = \begin{bmatrix} S_{11} & S_{12} & S_{16} \\ S_{21} & S_{22} & S_{26} \\ S_{61} & S_{62} & S_{66} \end{bmatrix} \begin{bmatrix} \sigma_1 \\ \sigma_2 \\ \sigma_6 \end{bmatrix} \quad (1)$$

The stress–strain relationship for an off-axis UD composite in terms of engineering constants is presented in Eq. (2),

$$\begin{bmatrix} \varepsilon_1 \\ \varepsilon_2 \\ \varepsilon_6 \end{bmatrix} = \begin{bmatrix} \frac{1}{E_1} & -\frac{\nu_{12}}{E_2} & \frac{\nu_{16}}{E_6} \\ -\frac{\nu_{21}}{E_1} & \frac{1}{E_2} & \frac{\nu_{26}}{E_6} \\ \frac{\nu_{61}}{E_1} & \frac{\nu_{62}}{E_2} & \frac{1}{E_6} \end{bmatrix} \begin{bmatrix} \sigma_1 \\ \sigma_2 \\ \sigma_6 \end{bmatrix} \quad (2)$$

Since the compliance matrix is symmetric,

$$S_{12} = S_{21}, S_{16} = S_{61}, S_{26} = S_{62} \quad (3)$$

The Poisson's ratio is not symmetric in its indices since the symmetry of the compliance leads to the following reciprocal relations,

$$\frac{\nu_{21}}{\nu_{12}} = \frac{E_1}{E_2} = \frac{S_{22}}{S_{11}}, \quad \frac{\nu_{61}}{\nu_{16}} = \frac{E_1}{E_6} = \frac{S_{66}}{S_{11}}, \quad \frac{\nu_{62}}{\nu_{26}} = \frac{E_2}{E_6} = \frac{S_{66}}{S_{22}} \quad (4)$$

The in-plane stress–strain relationship for a laminate is the stress resultant versus in-plane strain relation. The in-plane stress–strain relationship of symmetric laminates in terms of stiffness is offered in Eq. (5),

$$\begin{bmatrix} N_1 \\ N_2 \\ N_6 \end{bmatrix} = \begin{bmatrix} A_{11} & A_{12} & A_{16} \\ A_{21} & A_{22} & A_{26} \\ A_{61} & A_{62} & A_{66} \end{bmatrix} \begin{bmatrix} \varepsilon_1 \\ \varepsilon_2 \\ \varepsilon_6 \end{bmatrix} \quad (5)$$

where  $N$  and  $A$  are stress resultants and in-plane modulus matrix for an angle-ply composite laminate, respectively. Equation (5) is based on the laminate stiffness, and it is found by inverting the corresponding compliance as

$$a = A^{-1} \quad (6)$$

These stress–strain relationships are correct for the in-plane deformation of symmetric laminates. From the compliance in Eq. (6), effective engineering constants are calculated (where  $h$  is the total laminate thickness),

$$\begin{aligned} \text{In-plane effective longitudinal modulus} &= E_1^{\text{eff}} = \frac{1}{a_{11}h}, \\ \text{In-plane effective transverse modulus} &= E_2^{\text{eff}} = \frac{1}{a_{22}h}, \\ \text{In-plane effective shear modulus} &= E_6^{\text{eff}} = \frac{1}{a_{66}h}, \\ \text{In-plane effective Poisson's ratio} &= \nu_{21}^{\text{eff}} = -\frac{a_{21}}{a_{11}}, \quad \nu_{12}^{\text{eff}} = -\frac{a_{12}}{a_{22}}, \\ \text{In-plane effective shear coupling coefficient} &= \nu_{61}^{\text{eff}} = \frac{a_{61}}{a_{11}}, \quad \nu_{62}^{\text{eff}} = \frac{a_{62}}{a_{22}}, \\ \text{In-plane effective normal coupling coefficient} &= \nu_{16}^{\text{eff}} = \frac{a_{16}}{a_{66}}, \quad \nu_{62}^{\text{eff}} = \frac{a_{26}}{a_{66}} \end{aligned} \quad (7)$$

In the derivation of the stress–strain relationship of an angle-ply composite laminate, researchers such as Tsai and Hahn [28], Donoghue [30], and Evans [31] recognized the negative in-plane Poisson's ratio  $\nu_{21}$ , value in angle-ply laminates. Donoghue [30] calculated the variation of  $\nu_{21}$  with laminate off-axis angle for a range  $[\pm\theta]_s$ . He found that the negative in-plane Poisson's ratio arises between off-axis angles 35–50°. The maximum value was calculated for  $\theta = 25^\circ$  with a value of  $-0.245$  at an off-axis loading angle of  $40^\circ$ . These variations in the in-plane Poisson's ratio value of simple symmetrical laminates are clearly depicted in Fig. 1.

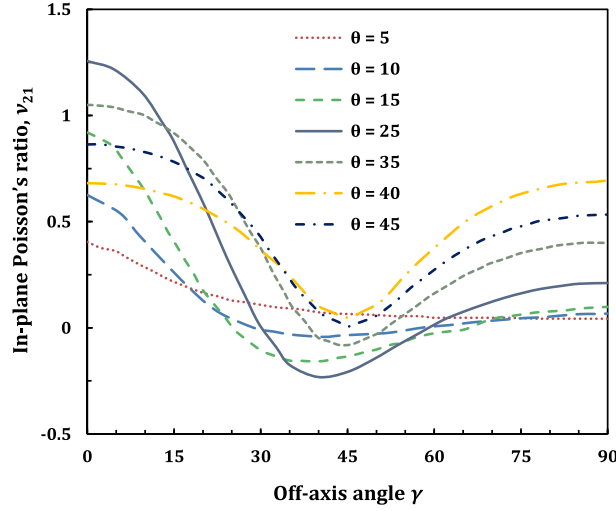


**Fig. 1** In-plane Poisson's ratio for various angle-ply laminates [30]

### 3 Negative out-of-plane Poisson's ratios, $v_{31}$ , laminates

General laminates lack midplane symmetry. They can either be antisymmetric or asymmetric. The CLT [28] has been extended to consider the out-of-plane effect [29]. For the laminate with voluntary layup, the relationship between load and deformation is written as,

$$\begin{Bmatrix} N \\ M \end{Bmatrix} = \begin{bmatrix} A & B \\ B & D \end{bmatrix} \begin{Bmatrix} \varepsilon \\ \kappa \end{Bmatrix} \quad (8)$$

where  $M$ ,  $A$ ,  $D$ ,  $B$ , and  $\kappa$  are moment, extension modulus matrix, flexural modulus matrix, coupling modulus matrix, and curvature for an angle-ply composite laminate, respectively. We have

$$\varepsilon = aN - aB\kappa \quad (9)$$

where  $a$  is the corresponding compliance matrix to the extension modulus matrix.

$$M = BaN + (D - BaB)\kappa \quad (10)$$

Equations (9) and (10) can be shown in a tabular form

$$\begin{Bmatrix} \varepsilon \\ M \end{Bmatrix} = \begin{bmatrix} a & -aB \\ Ba & D - BaB \end{bmatrix} \begin{Bmatrix} N \\ \kappa \end{Bmatrix} \quad (11)$$

The relationship in Eq. (11) is a partial inversion of that in Eq. (8). To derive the complete inversion, from Eq. (11) we have

$$\kappa = -(D - BaB)^{-1} BaN + (D - BaB)^{-1} M \quad (12)$$

$$\varepsilon = [a + aB(D - BaB)^{-1} Ba]N - aB(D - BaB)^{-1} M \quad (13)$$

According to Eqs. (11), (12), and (13) can be rewritten in a tabular form,

$$\begin{Bmatrix} \varepsilon \\ \kappa \end{Bmatrix} = \begin{bmatrix} a + aB(D - BaB)^{-1} Ba & -aB(D - BaB)^{-1} \\ -(D - BaB)^{-1} Ba & (D - BaB)^{-1} \end{bmatrix} \begin{Bmatrix} N \\ M \end{Bmatrix} \quad (14)$$

If there is no bending moment applied to the laminate, then we can get the expression of the strain vector,

$$\varepsilon = (a + aB(D - BaB)^{-1} Ba)N = \alpha N \quad (15)$$

where,

$$\varepsilon = \varepsilon_i = \{ \varepsilon_1 \ \varepsilon_2 \ \varepsilon_3 \ \varepsilon_6 \}^T,$$

$$\mathbf{N} = N_i = \{ N_1 \ N_2 \ N_3 \ N_6 \}^T \quad (16)$$

$$\mathbf{A} = A_{ij} = \begin{bmatrix} A_{11} & A_{12} & A_{13} & A_{16} \\ A_{12} & A_{22} & A_{23} & A_{26} \\ A_{13} & A_{23} & A_{33} & A_{36} \\ A_{16} & A_{26} & A_{36} & A_{66} \end{bmatrix}, \quad \mathbf{B} = B_{ij} = \begin{bmatrix} B_{11} & B_{12} & B_{13} & B_{16} \\ B_{12} & B_{22} & B_{23} & B_{26} \\ B_{13} & B_{23} & B_{33} & B_{36} \\ B_{16} & B_{26} & B_{36} & B_{66} \end{bmatrix},$$

$$\mathbf{D} = D_{ij} = \begin{bmatrix} D_{11} & D_{12} & D_{13} & D_{16} \\ D_{12} & D_{22} & D_{23} & D_{26} \\ D_{13} & D_{23} & D_{33} & D_{36} \\ D_{16} & D_{26} & D_{36} & D_{66} \end{bmatrix} \quad (17)$$

The out-of-plane coefficients are included in in-plane modulus matrix  $\mathbf{A}$ , coupling modulus matrix  $\mathbf{B}$ , and flexural modulus matrix  $\mathbf{D}$  of the composite, then the out-of-plane effective Poisson's ratios are derived as

$$\nu_{31}^{\text{eff}} = -\frac{\alpha_{31}}{\alpha_{11}}, \quad \nu_{32}^{\text{eff}} = -\frac{\alpha_{32}}{\alpha_{22}} \quad (18)$$

The elements of the modulus matrixes  $\mathbf{A}$ ,  $\mathbf{B}$ , and  $\mathbf{D}$  in Eq. (17) are evaluated by applying the following integration

$$[A_{ij}, B_{ij}, D_{ij}] = \int_{-h/2}^{+h/2} Q_{ij}[1, z, z^2] dz \quad (19)$$

where  $Q_{ij}$  are off-axis modulus coefficients of the transformed on-axis modulus matrix  $\mathbf{Q}$  for  $i$ -th ply group. For general laminates, the lower and the upper limits are from  $-h/2$  to  $+h/2$ . This is different from the limits for the symmetric laminates from the midplane ( $z = 0$ ) to the top face of the plate where  $z = h/2$ . They are calculated from the on-axis modulus coefficients and the ply angle  $\theta$ ,

$$\begin{aligned} Q_{11} &= Q_{xx} \cos^4 \theta + (2Q_{xy} + 4Q_{ss}) \cos^2 \theta \sin^2 \theta + Q_{yy} \sin^4 \theta, \\ Q_{22} &= Q_{yy} \cos^4 \theta + (2Q_{xy} + 4Q_{ss}) \cos^2 \theta \sin^2 \theta + Q_{xx} \sin^4 \theta, \\ Q_{33} &= Q_{zz}, \\ Q_{66} &= (Q_{xx} + Q_{yy} - 2Q_{xy} - 2Q_{ss}) \cos^2 \theta \sin^2 \theta + Q_{ss}(\sin^4 \theta + \cos^4 \theta), \\ Q_{12} &= (Q_{xx} + Q_{yy} - 4Q_{ss}) \cos^2 \theta \sin^2 \theta + Q_{xy}(\sin^4 \theta + \cos^4 \theta), \\ Q_{13} &= Q_{xz} \cos^2 \theta + Q_{yz} \sin^2 \theta, \\ Q_{16} &= (Q_{xx} - Q_{xy} - 2Q_{ss}) \cos^3 \theta \sin \theta + (Q_{xy} - Q_{yy} - 2Q_{ss}) \cos \theta \sin^3 \theta, \\ Q_{23} &= Q_{yz} \cos^2 \theta + Q_{xz} \sin^2 \theta, \\ Q_{26} &= (Q_{xx} - Q_{xy} - 2Q_{ss}) \cos \theta \sin^3 \theta + (Q_{xy} - Q_{yy} + 2Q_{ss}) \cos^3 \theta \sin \theta, \\ Q_{36} &= (Q_{xz} - Q_{yz}) \cos \theta \sin \theta \end{aligned} \quad (20)$$

The compliance matrix,  $\mathbf{S}$ , for an off-axis UD composite in terms of engineering constants is presented in Eq. (21),

$$\mathbf{S} = \begin{bmatrix} \frac{1}{E_1} & -\frac{\nu_{12}}{E_2} & -\frac{\nu_{13}}{E_3} & \frac{\nu_{16}}{E_6} \\ -\frac{\nu_{21}}{E_1} & \frac{1}{E_2} & -\frac{\nu_{23}}{E_3} & \frac{\nu_{26}}{E_6} \\ -\frac{\nu_{31}}{E_1} & -\frac{\nu_{32}}{E_2} & \frac{1}{E_3} & \frac{\nu_{36}}{E_6} \\ \frac{\nu_{61}}{E_1} & \frac{\nu_{62}}{E_2} & \frac{\nu_{63}}{E_3} & \frac{1}{E_6} \end{bmatrix} \quad (21)$$

The modulus matrix  $\mathbf{Q}$  is the inverse of the compliance matrix

$$\mathbf{Q} = \mathbf{S}^{-1} \quad (22)$$

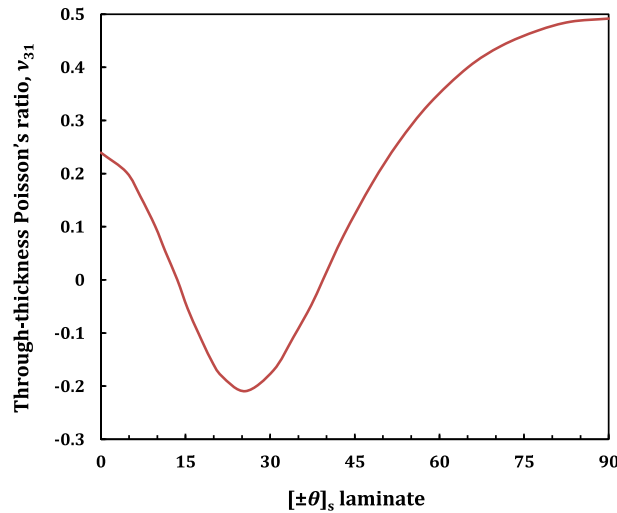


**Fig. 2** Through-thickness Poisson's ratios for angle-ply laminate [32]

Researchers such as Tsai and Hahn [28], Herakovich [32], Harkatie [33], and Coenen [34] have evaluated the existence of a negative through-thickness Poisson's ratio,  $\nu_{31}$ , in angle-ply laminates either analytically, numerically or experimentally. Herakovich [32] found the negative through-thickness Poisson's ratios are possible for a fiber orientation angle between 15 and 40°. At the ply angle of 25°, the largest negative through-thickness Poisson's ratio is found. Many laminate layups can achieve this effect. However, the number of 0-degree layers reduces the maximum negative Poisson's ratios and the orientation angles over which they occur. Herakovich [32] modeled laminates with negative  $\nu_{31}$  values by two-dimensional laminate theory and three-dimensional constitutive equations. The calculated through-thickness Poisson's ratio for the laminate with laminate off-axis angle for a range  $[\pm\theta]_s$  is illustrated in Fig. 2.

#### 4 Composite damage model

In general, there are two types of failure in composite laminates; laminar failure which includes matrix cracks and fiber breakage in compression and tension, and inter-laminar failure, which is due to the delamination of the laminate. Intra-laminar damage includes two parts; the initiation of damage, which is designated by one of the failure criteria, and damage progressive part, which can be linear or exponential. Also, inter-laminar failure includes two parts: onset of failure, which is designated by one of the inter-laminar failure criteria, and the damage progressive part, which is designated by energy-based methods.

##### 4.1 Damage model for a lamina

The damage behavior of the UD carbon fiber ply was considered with a user-defined material subroutine. The 3D Hashin damage failure criterion was utilized for the fiber failure modes, while the Puck criterion was specified for the matrix failure modes. This method was used since the Puck criterion has an improved prediction of matrix material damage for transverse compressive impact [35]. The relationships used to predict the initiation of fiber and matrix damage are as follows:

– Fiber tension:

$$r_{ft} = \left( \frac{\sigma_{xx}}{X_T} \right)^2 + \left( \frac{\sigma_{xy}}{S_{xy}} \right)^2 + \left( \frac{\sigma_{xz}}{S_{xz}} \right)^2, \sigma_{xx} > 0 \quad (23)$$

– Fiber compression:

$$r_{fc} = \frac{|\sigma_{xx}|}{X_C}, \sigma_{xx} < 0 \quad (24)$$

– Matrix tension:

$$r_{mt} = \left[ \left( \frac{\sigma_{xx}}{2X_T} \right)^2 + \frac{\sigma_{yy}^2}{|Y_T Y_C|} + \left( \frac{\sigma_{xy}}{S_{xy}} \right)^2 \right] + \sigma_{yy} \left( \frac{1}{Y_T} + \frac{1}{Y_C} \right), (\sigma_{xx} + \sigma_{yy}) > 0 \quad (25)$$

– Matrix compression:

$$r_{mc} = \left[ \left( \frac{\sigma_{xx}}{2X_T} \right)^2 + \frac{\sigma_{yy}^2}{|Y_T Y_C|} + \left( \frac{\sigma_{xy}}{S_{xy}} \right)^2 \right] + \sigma_{yy} \left( \frac{1}{Y_T} + \frac{1}{Y_C} \right), (\sigma_{xx} + \sigma_{yy}) < 0 \quad (26)$$

For a UD laminated composite, each ply is generally considered to be a transversely isotropic material. Thus, the stiffness matrix of such materials has five independent engineering constants. By defining different damage variables to consider material degradation during subsequent loading, the modified constitutive equations can be used to express the stress–strain relationship of the damaged ply. Therefore, the degraded stiffness matrix is shown in Eq. (27).

$$C_d = \frac{1}{\Delta} \times \begin{bmatrix} d_f E_{xx}(1 - d_m v_{yz} v_{zy}) & d_f d_m E_{xx}(v_{yx} + v_{yz} v_{zx}) & d_f E_{xx}(v_{zx} + d_f v_{yx} v_{zy}) & 0 & 0 & 0 \\ & d_m E_{yy}(1 - d_f v_{xz} v_{zy}) & d_m E_{yy}(v_{zy} + d_f v_{xy} v_{zx}) & 0 & 0 & 0 \\ & & E_{zz}(1 - d_f d_m v_{xy} v_{yx}) & 0 & 0 & 0 \\ & & & \Delta d_f d_m G_{xy} & 0 & 0 \\ \text{sym.} & & & & \Delta d_f d_m G_{yz} & 0 \\ & & & & & \Delta d_f d_m G_{xz} \end{bmatrix} \quad (27)$$

where  $d_f$  and  $d_m$  are defined as

$$\begin{cases} d_f = (1 - d_{ft})(1 - d_{fc}), \\ d_m = (1 - S_{mt} d_{mt})(1 - S_{mc} d_{mc}), \\ \Delta = 1 - d_f d_m v_{xy} v_{yx} - d_m v_{yz} v_{zy} - d_f v_{xz} v_{zx} - 2d_f d_m v_{yx} v_{zy} v_{xz} \end{cases} \quad (28)$$

where  $d_{ft}$ ,  $d_{fc}$ ,  $d_{mt}$ , and  $d_{mc}$  denote damage variables for the fiber and matrix in tensile and compression mode, respectively. The parameters  $d_{ft}$ ,  $d_{fc}$ ,  $d_{mt}$ , and  $d_{mc}$  are obtained by damage evolution methods. Also, coefficients  $S_{mt}$  and  $S_{mc}$  are introduced to eliminate element distortion related to shear stiffness degradation, their values are assumed as 0.9 and 0.5, respectively [36, 37].

Damage evolution defines the method where the stiffness of the laminate degrades after the damage is initiated. Now, the generally used damage evolution methods reduce the stiffness in the direction of damage growth due to the different damage modes, as a result, reducing the load-carrying capacity of the composite material. The equivalent-strain approach based on the critical fracture energy of the element used in this research is based on that of Li et al. [38], in which the damage variable is determined as

$$d_i = \frac{\varepsilon_{eq,i}^f (\varepsilon_{eq,i} - \varepsilon_{eq,i}^0)}{\varepsilon_{eq,i}^f (\varepsilon_{eq,i}^f - \varepsilon_{eq,i}^0)} \quad (29)$$

where  $i$  denotes the four different modes of damage (compressive and tensile damage of the matrix and fiber). Also,  $\varepsilon_{eq,i}$ ,  $\varepsilon_{eq,i}^0 = X_i/E_{0,j}$ , and  $\varepsilon_{eq,i}^f = 2G_i/(X_i l_c)$  are the equivalent strain, initial failure strain, and final failure strain, respectively. Furthermore,  $E_{0,j}$  is the initial modulus of the composite ply in the corresponding direction,  $X_i$  is the matrix or fiber strength,  $G_i$  is the critical fracture energy of the material, and  $l_c$  is the characteristic length of the element. The characteristic length is adopted to eliminate the mesh correlation in the FEM, which is in the direction along the crack propagation.

#### 4.2 Damage model for the interface

This research used a cohesive method based on damage mechanics and the bi-linear traction–separation law to simulate the interlaminar damage of composite laminates. The interlaminar damage model consists of damage initiation and evolution criteria. Interface damage was initiated once the function of the quadratic stress failure criteria reached 1.0 [39], which is shown in Eq. (30):

$$\left\{ \frac{\langle t_n \rangle}{t_n^0} \right\}^2 + \left\{ \frac{t_s}{t_s^0} \right\}^2 + \left\{ \frac{t_t}{t_t^0} \right\}^2 = 1 \quad (30)$$



**Table 1** Mechanical and strength properties of T700GC/M21 UD-ply [42]

Property		Values
Composite lamina	Density	$\rho = 1600 \text{ kg/m}^3$
	Modulus	$E_{xx} = 130 \text{ GPa}, E_{yy} = E_{zz} = 7.7 \text{ GPa},$ $G_{xy} = G_{xz} = 4.8 \text{ GPa}, G_{yz} = 3.8 \text{ GPa}$
	Poisson's ratio	$\nu_{xy} = \nu_{xz} = 0.33, \nu_{yz} = 0.35$
	Strength	$X_T = 2080 \text{ MPa}, X_C = 1250 \text{ MPa},$ $Y_T = 60 \text{ MPa}, Y_C = 140 \text{ MPa},$ $S_{xy} = S_{xz} = S_{yz} = 110 \text{ MPa}$
	Fracture energy	$G_{ft} = 133 \text{ N/mm}, G_{fc} = 40 \text{ N/mm},$ $G_{mt} = 0.6 \text{ N/mm}, G_{mc} = 2.1 \text{ N/mm}$
Interface	Modulus	$E = 5 \text{ GPa}$
	Strength	$t_n^0 = t_s^0 = t_t^0 = 30 \text{ MPa}$
	Fracture energy	$G_n^C = 0.6 \text{ N/mm}, G_s^C = 2.1 \text{ N/mm}$

where  $t_n^0$ ,  $t_s^0$ , and  $t_t^0$  are interface normal strength and shear strength;  $t_n$ ,  $t_s$ , and  $t_t$  are normal and shear tractions, respectively. In this expression, the Macaulay bracket signifies that compressive stress states are excluded.

The evolution of interface damage adopts the Benzeggagh-Kenane (B-K) law [40], based on the fracture mechanics,

$$G_n^C + (G_s^C - G_n^C) \left\{ \frac{G_s}{G_t} \right\}^\eta = G^C \quad (31)$$

where  $G_n^C$  and  $G_s^C$  are the critical fracture energy in the normal and shear directions, respectively.  $G_s$  is the value of dissipated energy in the out-of-plane shear directions,  $G_t$  is the total dissipated energy for all three directions, and  $\eta$  is a material constant that is set to 1.45 [37].

## 5 Auxetic angle-ply composite laminates

Effective negative Poisson's ratio can be tailored by manipulating the individual ply layup orientations, which designates the anisotropy of individual ply and the strain mismatch between adjacent plies [41]. In the present work, to study the response of angle-ply CFRP composite laminates in impact loads, laminates including 8-ply pairs were considered symmetrically. Based on the presented CLT [28, 29], a MATLAB code was used to identify laminates layup with the highest negative in-plane and through-thickness Poisson's ratio values, which were expected to provide the greatest increase in low-velocity impact resistance. The material parameters of CFRP UD-lamina used to calculate the effective properties were adopted, according to Table 1.

Figure 3 shows the calculation results of in-plane 3a and through-thickness 3b Poisson's ratio of laminates in terms of  $\theta$  angle change from 0 to 90°. According to Fig. 3a, the arrangement  $[\theta_2/65_2/\theta_2/65_2]_s$  with  $\theta = 15^\circ$  yields the largest value of negative in-plane Poisson's ratio for symmetric laminates with 8-ply pairs. Similarly, the largest value of negative through-thickness Poisson's ratio for a symmetric laminate with 8-ply pairs was obtained by the layup  $[25_2/-25_2/25_2/-25_2]_s$  (Fig. 3b). In addition, two new configurations of angle-ply CFRP composite laminates were designed as multi-component composites that partially included both in-plane and through-thickness auxetic behavior. It should be noted that the new configurations have the same overall effective properties and are non-auxetic. Meanwhile, their partial properties, including Sects. 1 and 2, are different and auxetic because of the different stacking sequences of the ply pairs. Figure 4 shows the new configurations of angle-ply CFRP composite laminates. Layup schedules and effective properties of the auxetic and non-auxetic angle-ply CFRP composite laminates based on the new configurations are given in Table 2.

## 6 Numerical modeling of low-velocity impact

To investigate the effect of the effective negative Poisson's ratio on the low-velocity impact behavior of the angle-ply CFRP composite laminates, numerical modeling was done using the finite element method and the dynamic/explicit solver of ABAQUS software. The angle-ply CFRP composite laminates with the layups in

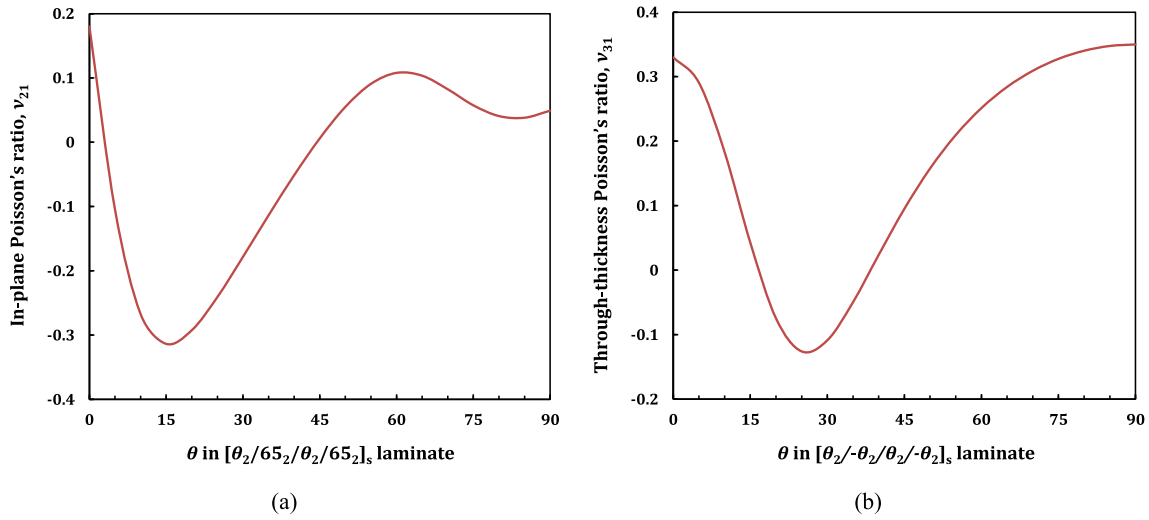


**Fig. 3** Predicted layups to create effective negative Poisson's ratios for angle-ply CFRP composite laminates **a** in-plane, and **b** through-thickness

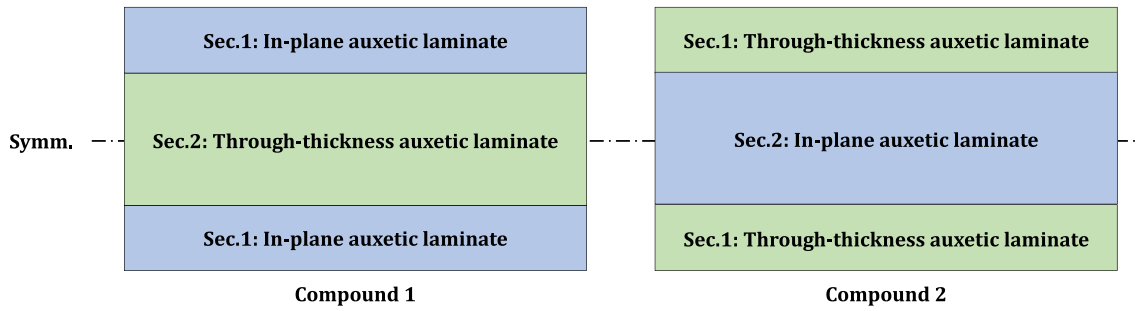


**Fig. 4** New configurations of multi-component compound angle-ply CFRP composite laminates

**Table 2** Layups and effective properties of the auxetic and the new configurations of multi-component compound laminates

Type	In-plane auxetic CFRP laminate	Through-thickness auxetic CFRP laminate	New multi-component configuration (Partial-auxetic CFRP laminate)	
			Compound 1	Compound 2
Layup	$[15_2/65_2/15_2/65_2]_s$	$[25_2/-25_2/25_2/-25_2]_s$	$[15_2/65_2/25_2/-25_2]_s$	$[25_2/-25_2/15_2/65_2]_s$
$\nu_{21}^{\text{eff}}$	-0.3137	1.4898	Sec. 1: -0.3137 Sec. 2: 1.4898 Total: 0.4548	Sec. 1: 1.4898 Sec. 2: -0.3137 Total: 0.4548
$\nu_{31}^{\text{eff}}$	0.4914	-0.1260	Sec. 1: 0.4914 Sec. 2: -0.1260 Total: 0.2412	Sec. 1: -0.1260 Sec. 2: 0.4914 Total: 0.2412
$E_1^{\text{eff}}$ (MPa)	40.95	63.31	68.18	68.18
$E_2^{\text{eff}}$ (MPa)	24.30	8.92	24.38	24.38
$E_3^{\text{eff}}$ (MPa)	8.10	8.10	8.42	8.42
$E_6^{\text{eff}}$ (MPa)	5.84	21.57	15.68	15.68

Table 2 and a geometry size of  $150 \times 100 \times 4$  mm are adopted. To simplify the model and enhance calculation efficiency, every two adjacent plies with the same ply orientation are treated as a single ply. Consequently, the final model has a total of eight layers, and the thickness of each ply is 0.5 mm. The VUMAT subroutine implements the progressive damage model of the angle-ply CFRP composite laminates. The material properties of the composite lamina in Table 1 are used as input in the simulation process.

To verify the FEM, the low-velocity impact test result reported by Hongkarnjanakul et al. [42] is used. The stacking sequence of the laminate used in the test by Hongkarnjanakul et al. [42] was  $[0_2/45_2/90_2/-45_2]_s$ .

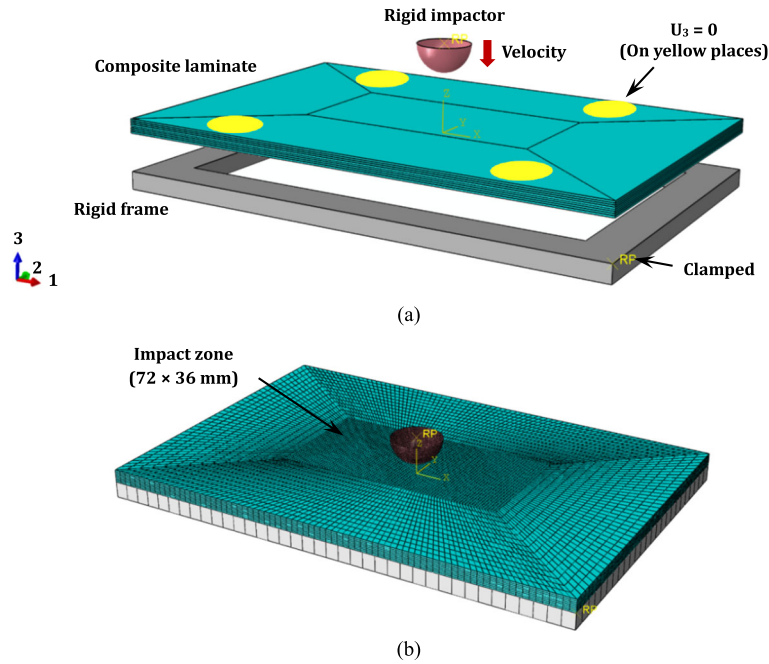


**Fig. 5** Composite laminate FEM for low-velocity impact analysis: **a** problem setup and boundary conditions, **b** model discretization

The experimental setup was done for a T700/M21 CFRP laminate panel using a drop-testing machine with an impactor weighing 2 kg and a diameter of 16 mm, according to the Airbus Industries Test Method (AITM 1–0010). The contact force between the laminate and the impactor was recorded by a piezoelectric power sensor inside the impactor. Also, the impactor’s velocity before impact was measured by an optical laser velocimeter. In the current study, the steel impactor is modeled as a rigid body with a hemispherical head with a diameter of 16 mm and a lumped reference mass of 2 kg. The impactor’s velocity is 5 m/s, representing an impact energy of 25 J. The composite laminate is placed on top of a rigid frame with an inner open-cut window of  $125 \times 75$  mm. All degrees of freedom of the rigid frame are clamped. To arrest large out-of-plane movement of the laminate, the displacement of the selected nodes in the 3-axis direction is constrained on the yellow places as shown in Fig. 5a to simulate the restrictions of the four rubber clamps in the test fixture. For the impactor, only the degree of freedom along the 3 direction is not constrained. This indicates that the FEM will be consistent with the experiment.

To apply the contact in the low-velocity impact between the impactor, the composite laminate, the rigid frame, and also ply-to-ply contact in the laminate, the general contact algorithm with the hard contact and the penalty method with a friction coefficient generally set as 0.3 [29, 37, 38] used to define the normal and tangential contact behaviors, respectively. The total simulation time takes 4 ms, and the stable incremental time is set to below  $1e - 4$  ms to obtain numerical convergence. To model the delamination, the interfaces between each adjacent ply pair are considered using cohesive surface contacts. The Benzeggagh and Kenane (B-K) delamination criterion [40] along with mixed-mode fracture energy law, are adopted to model the initiation and evolution of the delamination damage.

To have a numerical solution with accurate prediction, the mesh should be fine enough to predict well the dynamic progressive damage of a composite laminate without being computationally expensive. In the present work, for FEM discretization, the CFRP composite laminate is discretized into two regions: the refined center region of the mesh (impact region) and the coarser outer region (Fig. 5b). The mesh size at the center region ( $72 \times 36$  mm) under the impactor is refined to  $0.9 \times 0.9$  mm. In contrast, to reduce the computational time, the mesh at the regions far away from the impact site is adopted using a global seed size of 3.5 mm. The CFRP composite laminate is discretized using the C3D8R elements (i.e., An 8-node linear brick, reduced integration, hourglass control). While the impactor and the rigid frame are modeled as discrete rigid bodies and meshed with R3D4 elements (An 4-node 3-D bilinear rigid quadrilateral). The global seed sizes of the impactor and the rigid frame are created using a global seed size of 0.5 and 3 mm, respectively (Fig. 5b).

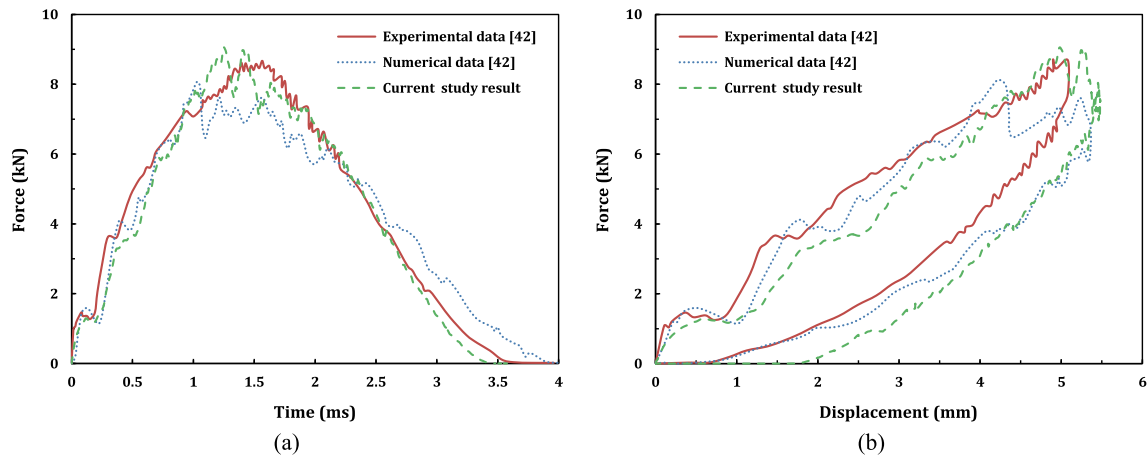


**Fig. 6** Verification of the low-velocity impact model: **a** impact force versus time history, **b** impact force versus displacement

## 7 Results and discussion

In previous research studies, auxetic laminates, both in-plane [5] and through-thickness [15] were compared and analyzed with their non-auxetic counterparts in low-velocity impact loading. The results indicated that in some cases of damage, auxetic laminates performed better, as compared to their non-auxetic counterparts. The present research aimed to simultaneously investigate and compare both in-plane and through-thickness auxetic laminates with each other, as well as studying the improvement in the impact damage behavior of composite laminates by using the new combined stacking sequences of both in-plane and through-thickness layups (Fig. 5). To achieve the maximum negative in-plane and through-thickness Poisson's ratio value, a MATLAB code was developed based on the relations of the CLT [28, 29], as presented in Sects. 2 and 3, the results of which are shown in Fig. 3. The layups were adopted according to Table 2. The properties of CFRP composite laminates and their interface, including density, elastic properties, strengths, and fracture energies, were considered according to Table 1. The results obtained in this study are related to a 2 kg impactor with a velocity of 5 m/s which the impact energy is equivalent to 25 J. This level of impact energy is suitable for studying delamination damage and matrix and fiber damage in a 16-ply CFRP composite laminate.

### 7.1 Model verification results

The numerical results, including impact force–time and impact force–displacement curves, have been compared with the experimental tests and other valid numerical models to verify the numerical model. For this purpose, experimental test data and the numerical model of Hongkarnjanakul et al. [42] were used. According to Fig. 6a, the predicted impact force history including the peak load, the time to peak load, and the impact duration were in good agreement with the experimental data. Also, a comparison of the impact force–displacement curves in Fig. 6b shows that the overall impact behavior agreed with the experimental data.

In addition, the delamination damage patterns between the numerical model results of the present study were compared with the experimental test results obtained by Hongkarnjanakul et al. [42] (Fig. 7a). Additionally, the numerical model's results of Li et al. [38] and Wang [15] were also compared (Fig. 7b). In general, the low-velocity impact numerical model and the VUMAT subroutine calculation algorithm were well capable of predicting the initiation and evolution of damage for matrix, fiber, and delamination. The results were confirmed to be accurate in predicting the progressive damage and delamination caused by a low-velocity impact on a composite laminate. After verification of the FEM for the low-velocity impact, it was utilized to examine the effect of negative in-plane and through-thickness Poisson's ratio of composite laminates.

### 7.2 Global low-velocity impact response

Figure 8 shows the overall low-velocity impact response of the auxetic laminates and new configurations. According to Fig. 8a, at the time range of 0.15 ms, the tensile damage of the matrix is initiated, as a result of

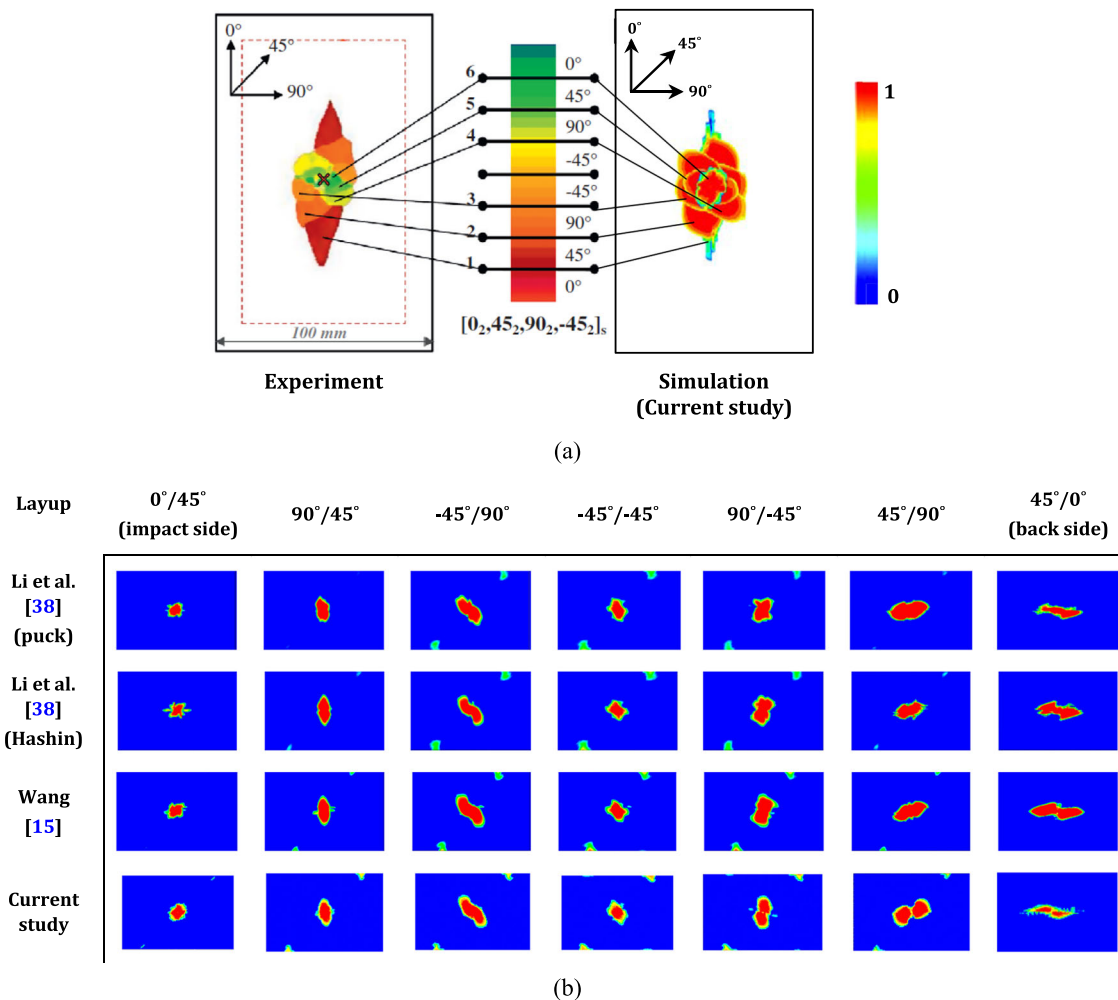


**Fig. 7** Verification of the low-velocity impact model: **a** overlapped delamination area (experimental data were obtained using ultrasonic C-scan [42]), **b** comparisons between numerical models results

which the stiffness of the material is degraded and the impact force is reduced. After the time  $t = 0.2$  ms with progressive impactor into the composite laminate, the impact force increases until reaching the approximate time  $t = 0.4$  ms. At this time, the compressive damage of the matrix is initiated, which causes the degradation of the laminate stiffness. In the following, a decreasing trend in the growth rate in the impact force is shown, which is caused by a further decrease in the material stiffness due to the propagation of tensile and compressive damage of the matrix. The approximate time  $t = 0.75$  ms is where the tensile and compressive damage of the matrix is propagated to most of the plies, which causes stiffness degradation in other plies, and as a result, the impact force is reduced. Following the more progressive impactor, and the increase of the impact force applied to the composite laminate, the tensile and compressive damage of the matrix propagates. Also, the tensile damage of the fiber initiated at the time range of  $t = 1.2$  ms, which results in further degradation of the material stiffness. When the impactor reaches the lowest position in the time range of  $t = 1.8$  ms, it rebounds. Meanwhile, the out-of-plane displacement of the laminate recovers gradually, and the composite laminate damage continues to propagate for a certain period at a much lower rate than before. It should be noted that the time ranges of the in-plane auxetic laminate are somewhat different from those of other laminates.

According to Fig. 8b, the in-plane auxetic laminate shows the lowest value of impact force. Meanwhile, the laminates with the new configurations exhibit a higher impact force, as compared to their auxetic counterparts. The impact force of the laminates with the new configurations is 35% and 8% more than that of in-plane and through-thickness auxetic ones, respectively. Mechanical impact is a contact problem in which the effective contact modulus is a function of the through-thickness modulus [29]. Also, impact includes biaxial bending in

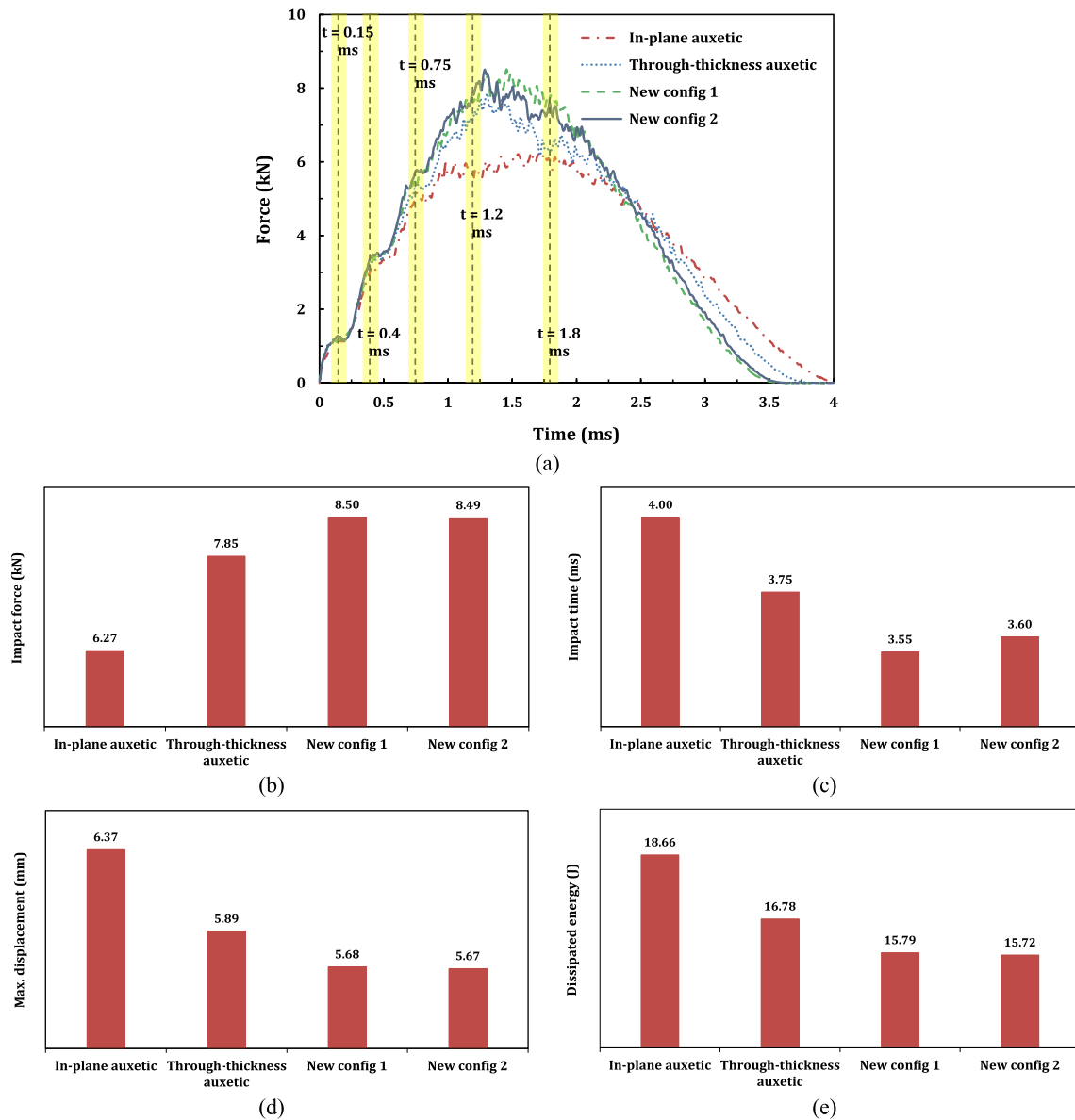


**Fig. 8** Comparison of the global impact response between the auxetic and new configurations CFRP composite laminates: **a** impact force versus time history, **b** impact force, **c** impact time, **d** maximum displacement, and **e** dissipated energy

which transverse stiffness also performs an important role [15]. Therefore, the higher impact force of laminates with the new configurations, as compared to the auxetic ones, is due to the larger effective longitudinal, transverse, and through-thickness moduli. Also, due to the larger size of the composite laminate in the  $x$  direction, the effective longitudinal modulus is more important. In particular, the impact force of the through-thickness auxetic laminate is 25% more than that of the in-plane auxetic one, which is due to its higher effective longitudinal modulus. Meanwhile, the effective transversal modulus of the through-thickness auxetic laminate is lower than that of the in-plane auxetic one. According to Fig. 8c, auxetic laminates show a longer impact time than those with the new configurations. Meanwhile, the in-plane auxetic laminate has the highest impact time, and the new laminate configuration 1 has the lowest impact time, which indicates a difference of more than 12%. In this regard, Wang [15] showed that the through-thickness auxetic laminate has a shorter impact time than non-auxetic configurations  $[50_2/0_2/50_2/0_2/50_2]$  and  $[20_2/10_2/5_2/10_2/20_2]$ . However, the laminates with the new configurations introduced in this research have a shorter impact time than the through-thickness auxetic laminate. As shown in Fig. 8d, the laminates with the new configurations have a lower maximum

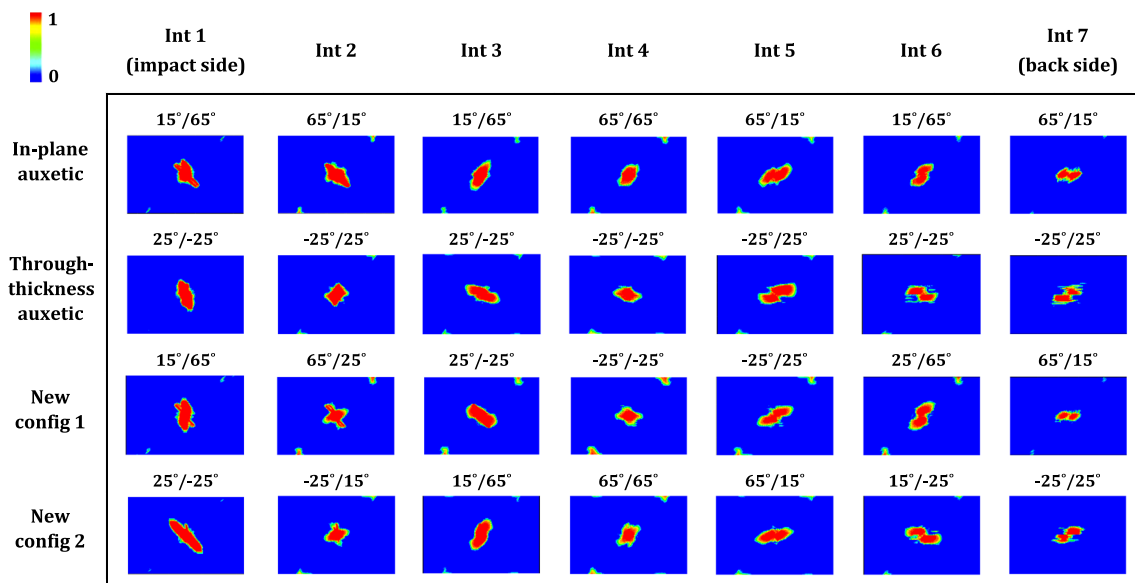


**Fig. 9** Comparison of predicted delamination damage in each interface of the auxetic and new configurations CFRP laminates (The contour plots from left to right show the delamination damage patterns in each interface of the composite laminate. Also the red color indicates complete delamination damage while the blue color indicates no delamination damage.)

displacement value than their auxetic counterparts due to their higher effective moduli. Meanwhile, the in-plane auxetic laminate has the highest maximum displacement value, which is more than 12% higher than that of laminates with the new configurations.

Dissipated energy is related to the damage behavior of composite laminates. The values of dissipated energy are shown in Fig. 8e, based on which laminates with the new configurations show less dissipated energy than the auxetic ones. The highest value of dissipated energy is related to the in-plane auxetic laminate, while the lowest one is related to the new laminate configuration 2 with more than 18% difference, as compared to the in-plane auxetic laminate one. In general, the investigation of the results of the mechanical response of the studied laminates shows that the in-plane auxetic laminate with a behavior involving low impact force, high impact time, and high maximum displacement is useful in sacrificial structures for the protection and safety of humans. Meanwhile, laminates with the new configurations have features such as high impact force, low impact time, and low maximum displacement that are applicable in structures with the hardwall design approach.

### 7.3 Delamination damage

Figure 9 shows the predicted delamination patterns at each interface of the composite laminates. The colors blue and red represent undamaged and fully damaged areas, respectively. Also, to further investigate the effect of negative Poisson's ratio on delamination damage, a quantitative comparison of the delamination damage of the central area of each interface of the composite laminates is given in Fig. 10. The calculated areas are for elements whose damage variable is greater than 0.5. The results show that for the third to seventh interfaces, as well as some of the first and second ones, the delamination propagation is approximately parallel to the fiber orientations of the ply below the corresponding interface. This is also consistent with the findings reported by references [5, 37, 38]. The delamination damage of the new configuration 1 in the upper and lower interfaces is 23.6% and 38.2% less than that of the new configuration 2, respectively. Meanwhile, in the second, third, fifth, and sixth interfaces, the new configuration 2 shows less delamination damage than the new configuration 1. Regarding the effect of the negative Poisson's ratio on delamination damage, Wang [15] reported that the presence of negative through-thickness Poisson's ratio, as well as the increase of the effective transverse modulus, can lead to the increase of propagation of delamination damage. Lin et al. [5] also stated that producing a negative in-plane Poisson's ratio can be useful to reduce the delamination damage areas at the top and bottom interfaces, especially at relatively higher impact energies.

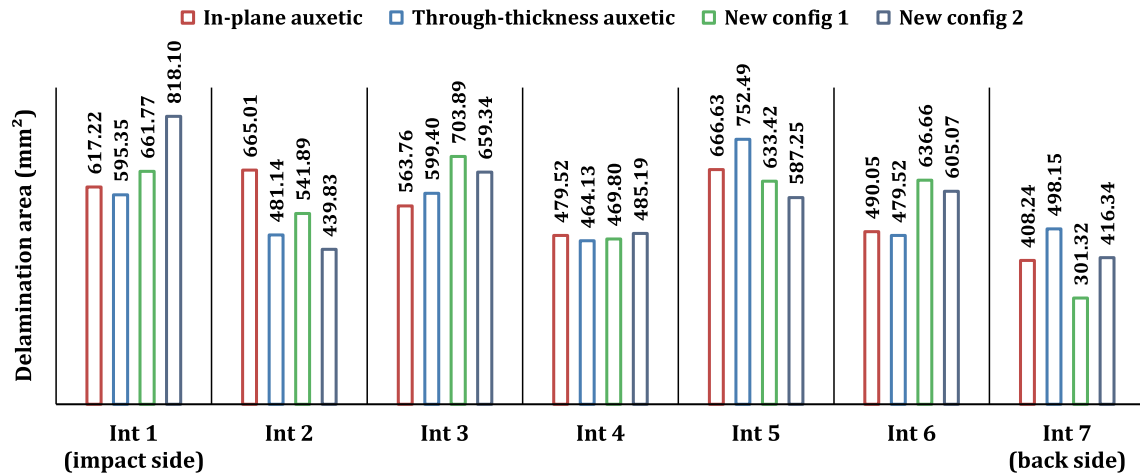


**Fig. 10** Comparison of predicted delamination damage areas in each interface of the auxetic and new configurations CFRP laminates

#### 7.4 Matrix and fiber damage

The damage modes of CFRP composite laminates under low-velocity impact often include matrix tension, matrix compressive, and fiber tension. In most cases, the compressive damage of fiber is ignored due to its insignificance [15, 38]. The predicted patterns of the matrix tensile damage of the auxetic laminates and the two new configurations are shown in Fig. 11. Also, for a better comparison, the quantitative values of the matrix tensile damaged areas are given in Fig. 12. In general, in a low-velocity impact problem on a flat plate, the impact force causes the bending of the plate, leading to tension on the back side and compression on the impact side of the plate. Therefore, for the studied composite laminates, the matrix tensile damage is initiated from the back side and propagation to the impact side which can be seen in the matrix tensile damage patterns in Fig. 11 and the quantitative data given in Fig. 12. As can be seen in Fig. 11, the patterns of the matrix tensile damaged areas in the upper plies are localized damage in the impact zone, while in the lower ones, the damaged areas are often propagation along the fiber direction. Such patterns for matrix tensile damage are common for CFRP composite laminates under low-velocity impact [5, 38].

According to Figs. 11 and 12, a comparison of the matrix tensile damaged areas for in-plane and through-thickness auxetic laminates shows that through-thickness auxetic laminate, despite lower effective transverse modulus, has less matrix tensile damage in the first to fifth plies, as compared to in-plane auxetic laminate. However, in the lower three plies, these results do not hold. In this regard, Wang [15] showed that the production of negative through-thickness Poisson's ratio suppresses the propagation of the tensile damage of the matrix.

By comparing the predicted matrix tensile damage for auxetic laminates and the two new configurations, it was found that laminates with the new configurations had less matrix tensile damage than the auxetic ones. This is due to the higher effective transverse modulus of the new configurations, as compared to the auxetic ones. In addition, although the effective transverse modulus of the two new configurations and in-plane auxetic laminate is almost equal, the tensile damage of the matrix of the new configurations is significantly less than that of the in-plane auxetic one, which is due to the presence of the plies with fiber angle of  $\pm 25^\circ$  in laminates with the new configurations, which causes a local through-thickness auxetic behavior. A comparison of the matrix tensile damage of the new configurations 1 and 2, as can be seen in Fig. 12, shows that the predicted damage areas are slightly different in the two upper plies and also the sixth and seventh ones. Meanwhile, in the third, fourth, fifth, and eighth plies, the damaged areas are 39%, 27%, 26%, and 14% less for the new configuration 2, respectively. In general, based on the investigations, both the higher effective transverse modulus and the negative through-thickness Poisson's ratio are influential in reducing the tensile damage of the matrix. These results are also consistent with the findings reported by Wang [15].

The results obtained from the prediction of matrix compression damage patterns, as well as the corresponding damaged areas, are shown in Figs. 13 and 14. Unlike the tensile damage of the matrix, the compressive damage of the matrix gradually decreases from the impact side to the back side, which is consistent with the results reported by Ref. [38]. Based on Figs. 13 and 14, a comparison of the matrix compression damaged areas for in-plane and through-thickness auxetic laminates shows that in the first and second plies, matrix



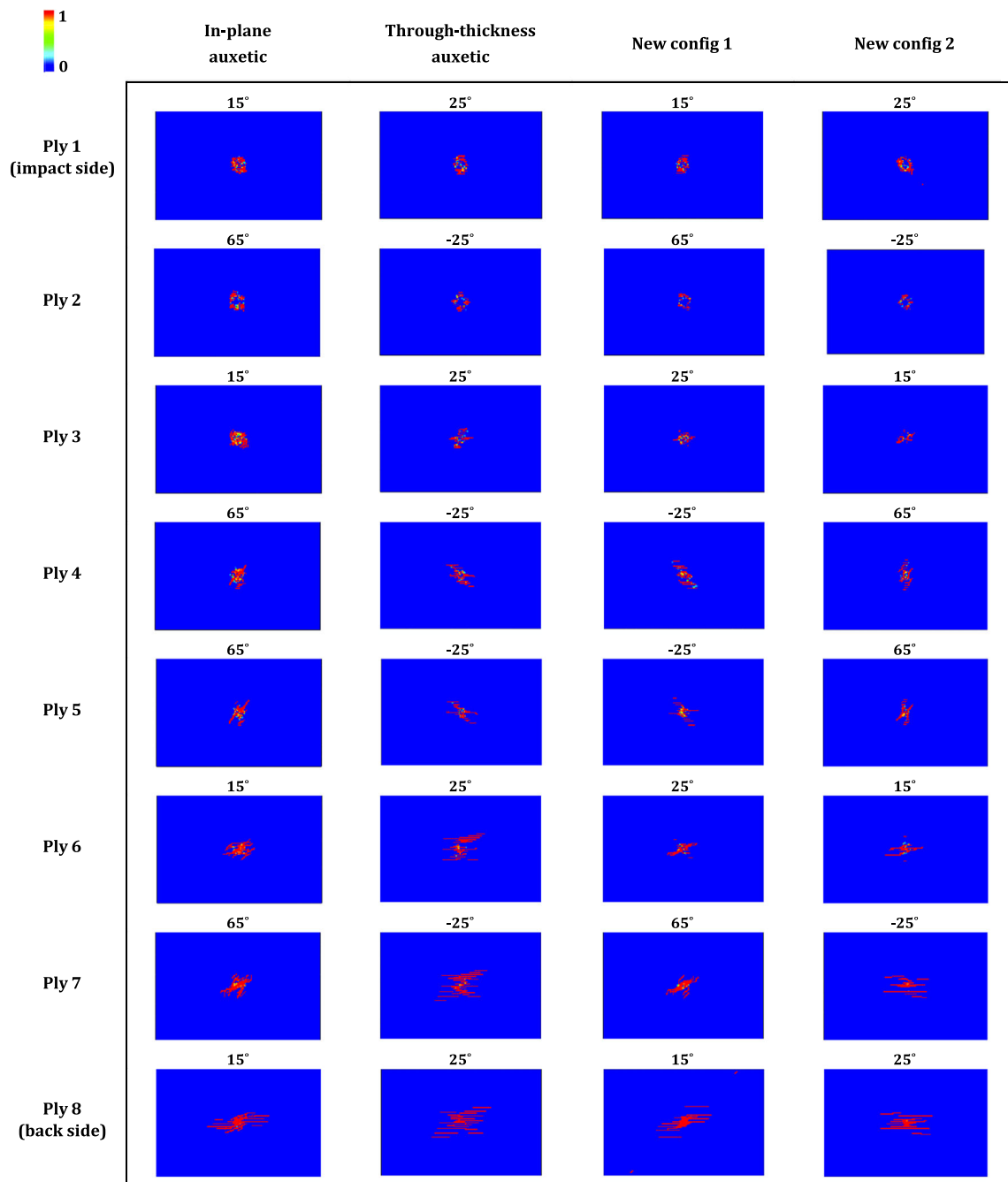


**Fig. 11** Comparison of predicted matrix tensile damage in each ply of the auxetic and new configurations CFRP laminates (The contour plots from up to down show the matrix tensile damage patterns in each ply of the composite laminate. The red color indicates complete matrix tensile damage while the blue color indicates no matrix tensile damage.)

compression damage is more for the through-thickness auxetic laminate. Meanwhile, in other plies, the compression damage of the matrix is less for through-thickness auxetic laminate. In particular, the compressive damage of the matrix for the through-thickness auxetic laminate in the third and fourth plies is 58.3% and 58.6% higher, respectively, as compared to their in-plane auxetic counterpart. Also, the compressive damage of the matrix for the through-thickness auxetic laminate in the first and second plies are 26.2% and 17.8% higher than that of the new configuration 1 laminate, respectively. In this regard, Wang [15] reported that the through-thickness auxetic behavior could unfavorably extend the compressive damaged areas of the matrix, as

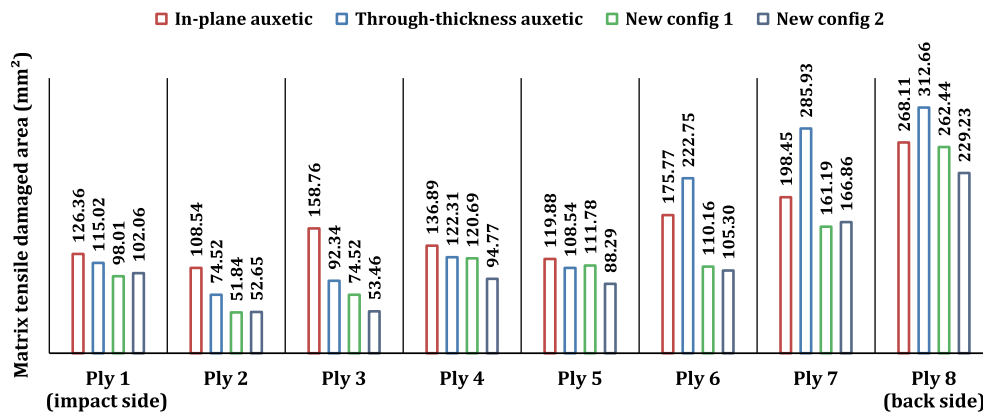


**Fig. 12** Comparison of predicted matrix tensile damage area in each ply of the auxetic and new CFRP laminates configurations

compared to the non-auxetic laminates. This could be due to the laminate contraction during the impact event caused by the negative Poisson's ratio, which exacerbates the compressive damage of the matrix. In general, the results indicate that in most of the plies and, especially, in the upper ones, the compression damage of the matrix is less for laminates with the new configurations than for their auxetic counterparts. A comparison of the predicted results of matrix compressive damage for the two new configurations shows that new configuration 1 has less damage than the new configuration 2 in the upper plies; however, this is not true in the lower ones, especially in the seventh one.

Fiber tensile damage patterns of the auxetic laminates and the two new configurations are shown in Fig. 15. As can be seen, the tensile damage of the fiber initiated from the impact side and propagation to the back side, from the third ply onwards, the tensile damage of the fiber in composite laminates is insignificant or without damage. According to Fig. 16, the predicted areas for fiber tensile damage are much smaller than those for other damage modes. In general, for a low-velocity impact problem, fiber damage is rarely observed [38]. A comparison of values of fiber tensile damage area, as represented in Fig. 16, the through-thickness auxetic laminate in the first and third plies, as well as new configurations 2 in the second and fourth ones, shows the highest tensile damage of the fiber.

## 8 Conclusion

Auxetic laminates are a promising solution to improve mechanical properties subjected to impact loading. The layups of plies can be oriented to achieve negative in-plane or through-thickness Poisson's ratio behavior, each of which has its unique properties. This research examines the damage behavior of both in-plane and through-thickness auxetic composite laminates, as well as two new configurations whose stacking sequences are a new combination of in-plane and through-thickness auxetic layups. The results indicate that combining in-plane and through-thickness auxetic layups can lead to the improvement of the mechanical properties and the reduction of the damage to the composite laminates. The most important benefits include:

- Increasing the effective moduli: a comparison of the effective modulus of composite laminates shows that the effective longitudinal, transverse, and through-thickness moduli of laminates with the new configurations are higher than those of auxetic laminates, which improves the mechanical response and also reduces the damage in the respective laminates.
- Improving the overall low-velocity impact response: The results indicate that the new configurations 1 and 2 have features such as high impact force, low impact time, and low maximum displacement, which makes them suitable for usage in structures with a hardwall design approach.
- Damage reduction: The predicted dissipated energy values indicate that laminates with the new configurations exhibit less dissipated energy than their auxetic counterparts, which indicates their overall lower damage. Also, the predicted areas of delamination damage, tension damage, and compression damage of the matrix and fiber tension damage show that in most cases, the damage of laminates with the new configurations is less than that of the auxetic ones.
- Identification of the unique behavior of the in-plane auxetic laminate: The general response of the low-velocity impact on the in-plane auxetic laminate indicates that this composite laminate with features such

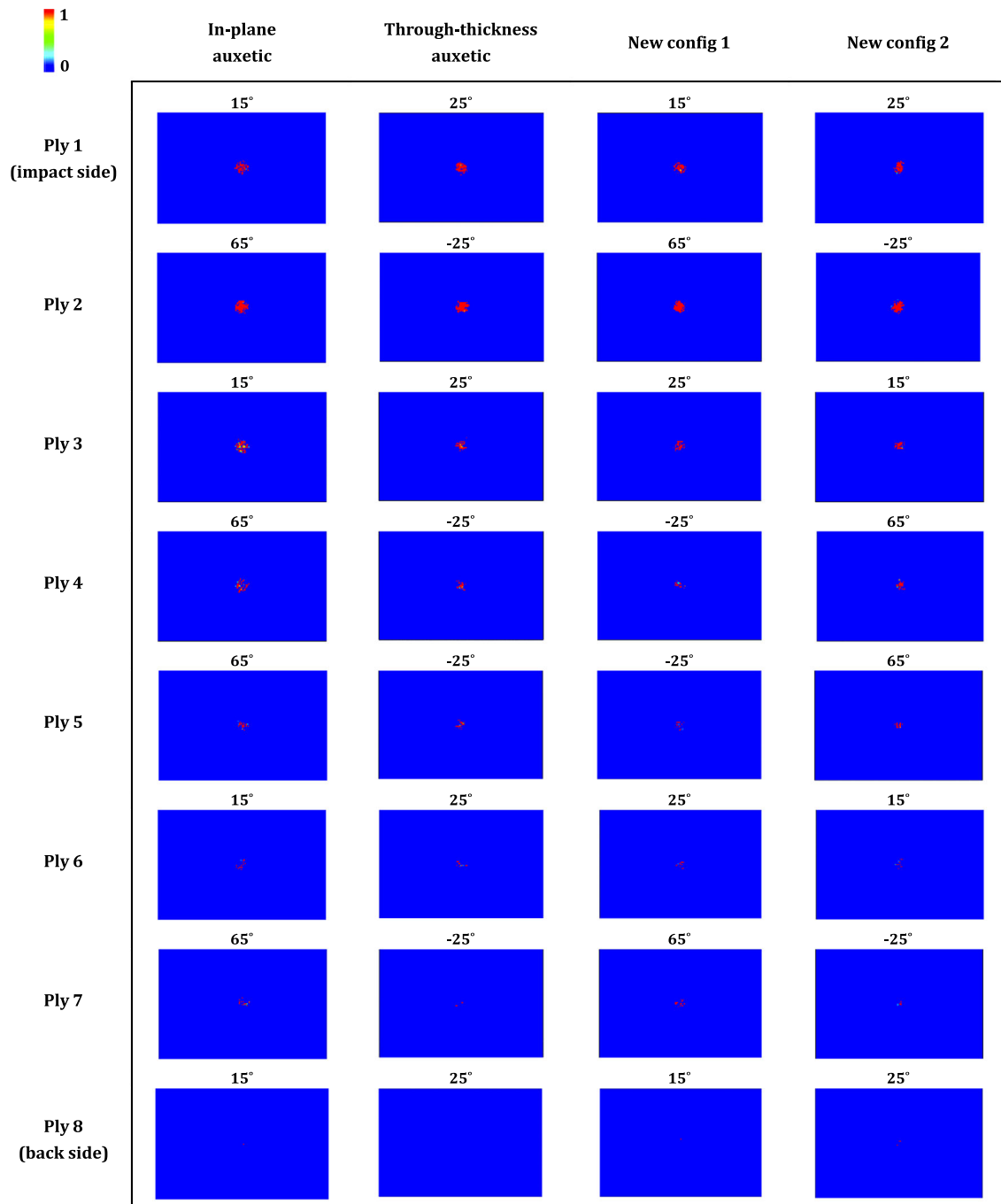


**Fig. 13** Comparison of predicted matrix compression damage in each ply of the auxetic and new CFRP laminates configurations (The contour plots from up to down show the matrix compression damage patterns in each ply of the composite laminate. The red color indicates complete matrix compression damage, while the blue color indicates no matrix compression damage.)

as low impact force, high impact time, and high maximum displacement, as compared to other laminates studied in this research, can be developed for usage in sacrificial structures for the protection and safety of humans.

**Author contribution** Reza Sareman: Formal analysis, Investigation, Methodology, Resources, Software, Writing—original draft. Majid Jamal- Omid: Conceptualization, Data curation, Methodology, Project administration, Supervision, Validation, Writing—review and editing. Jamasb Pirkandi: Conceptualization, Data curation, Formal analysis, Methodology, Resources.

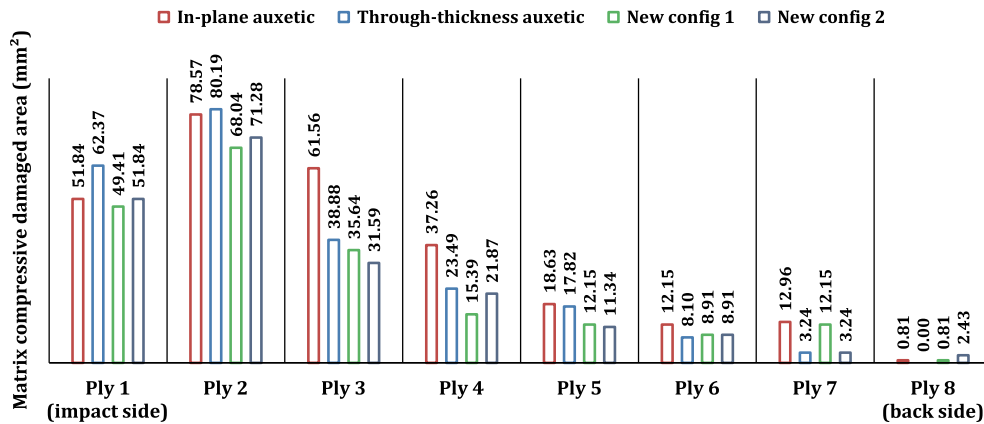


Fig. 14 Comparison of predicted matrix compression damage area in each ply of the auxetic and new CFRP laminates configurations

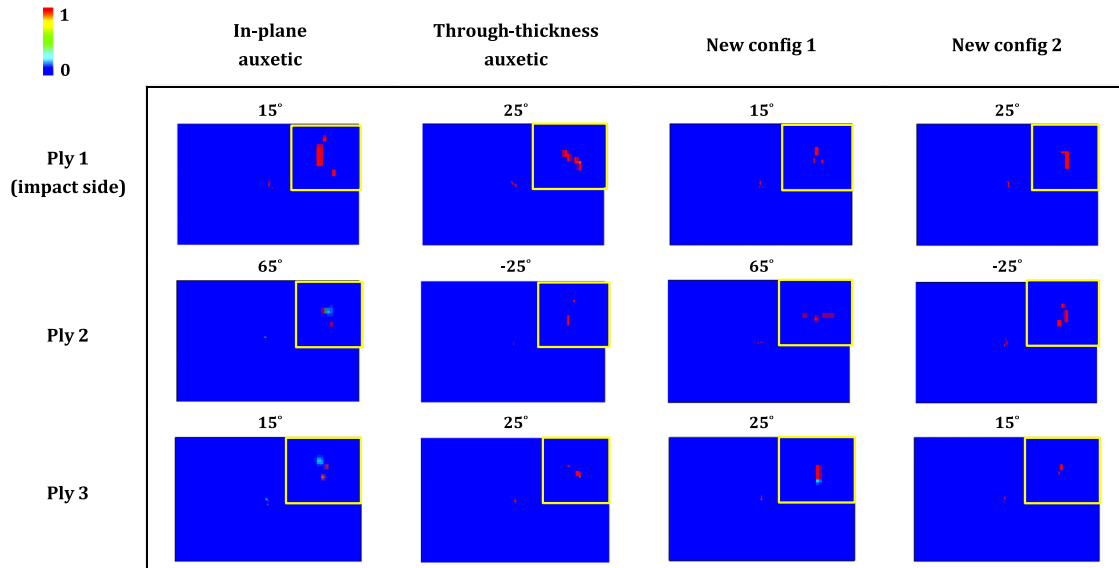


Fig. 15 Comparison of predicted fiber tensile damage in each ply of the auxetic and new CFRP laminates configurations (The contour plots from up to down show the fiber tensile damage patterns at each ply of the composite laminate. The red color indicates complete fiber tensile damage while the blue color indicates no fiber tensile damage.)

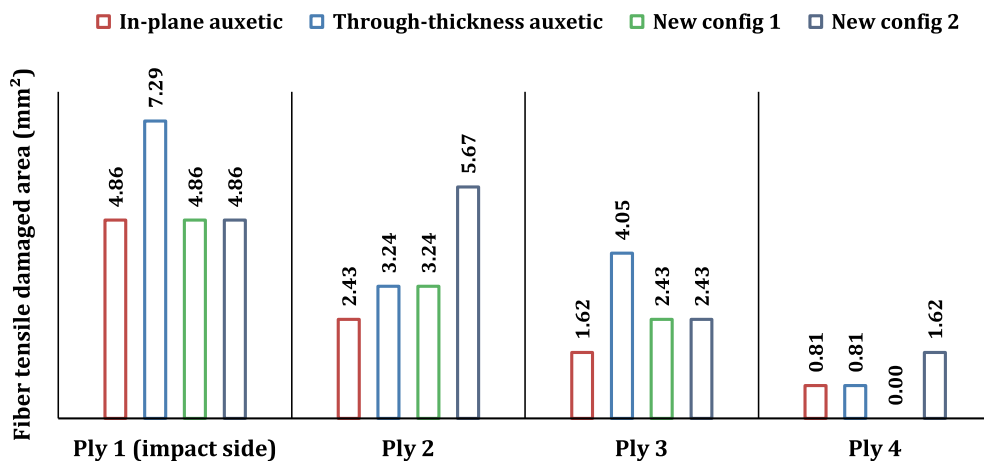


Fig. 16 Comparison of predicted fiber tensile damage area in each ply of the auxetic and new configurations CFRP laminates

**Data availability** No datasets were generated or analyzed during the current study.

## Declarations

**Conflict of interest** It is declared that there is no conflict of interest in this research work.

**Compliance with ethical standards** There is no ethical concern in this research work.

## References

1. Rajak, D.K., Pagar, D.D., Menezes, P.L., Linul, E.: Fiber-reinforced polymer composites: manufacturing, properties, and applications. *Polymers* **11**, 1667 (2019). <https://doi.org/10.3390/polym11101667>
2. Vidal, P., Gallimard, L., Polit, O.: Local refinement for the modeling of composite beam based on the partition of the unity method. *Finite Elem. Anal. Des.* **230**, 104100 (2024). <https://doi.org/10.1016/j.finel.2023.104100>
3. Fortuna, B., Turk, G., Schnabl, S.: A new locking-free finite element for N-layer composite beams with interlayer slips and finger joints. *Finite Elem. Anal. Des.* **220**, 103936 (2023). <https://doi.org/10.1016/j.finel.2023.103936>
4. Sharma, A.K., Bhandari, R., Sharma, C., Dhakad, S.K., Pinca-Bretotean, C.: Polymer matrix composites: a state of art review. *Mater. Today Proc.* **57**, 2330–2333 (2022). <https://doi.org/10.1016/j.matpr.2021.12.592>
5. Lin, W., Wang, Y.: Low velocity impact behavior of auxetic CFRP composite laminates with in-plane negative poisson's ratio. *J. Compos. Mater.* **57**, 2029–2042 (2023). <https://doi.org/10.1177/00219983231168698>
6. Kim, D.-H., Kim, S.-W.: Process-induced distortion of triaxially braided composites considering different geometric parameters using simplified constitutive model with effective property. *Finite Elem. Anal. Des.* **222**, 103974 (2023). <https://doi.org/10.1016/j.finel.2023.103974>
7. Min, K., Oh, M., Kim, C., Yoo, J.: Topological design of thermal conductors using functionally graded materials. *Finite Elem. Anal. Des.* **220**, 103947 (2023). <https://doi.org/10.1016/j.finel.2023.103947>
8. Bouvet, C., Rivallant, S.: Damage tolerance of composite structures under low-velocity impact, In *Dynamic Deformation. Damage and Fracture in Composite Materials and Structures* (2023 Jan 1), pp. 3–28. Woodhead Publishing. <https://doi.org/10.1016/B978-0-12-823979-7.00002-8>
9. Jiang, W., Ren, X., Wang, S.L., Zhang, X.G., Zhang, X.Y., Luo, C., Xie, Y.M., Scarpa, F., Alderson, A., Evans, K.E.: Manufacturing, characteristics and applications of auxetic foams: a state-of-the-art review. *Compos. Part B Eng.* **235**, 109733 (2022). <https://doi.org/10.1016/j.compositesb.2022.109733>
10. Rana, S., Magalhães, R., Fanguero, R.: Advanced auxetic fibrous structures and composites for industrial applications. In: *Proceedings of the 7<sup>th</sup> International Conference on Mechanics and Materials in Design Albufeira/Portugal*, pp. 643–650 (2017)
11. Gomes, R.A., De Oliveira, L.A., Francisco, M.B., Gomes, G.F.: Tubular auxetic structures: a review. *Thin-Walled Struct.* **188**, 110850 (2023). <https://doi.org/10.1016/j.tws.2023.110850>
12. Li, K., Zhang, Y., Hou, Y., Su, L., Zeng, G., Xu, X.: Mechanical properties of re-entrant anti-chiral auxetic metamaterial under the in-plane compression. *Thin-Walled Struct.* **184**, 110465 (2023). <https://doi.org/10.1016/j.tws.2022.110465>
13. Pan, Y., Zhang, X.G., Han, D., Li, W., Xu, L.F., Zhang, Y., Jiang, W., Bao, S., Teng, X.C., Lai, T., Ren, X.: The out-of-plane compressive behavior of auxetic chiral lattice with circular nodes. *Thin-Walled Struct.* **182**, 110152 (2023). <https://doi.org/10.1016/j.tws.2022.110152>
14. Yu, S., Liu, Z., Cao, X., Liu, J., Huang, W., Wang, Y.: The compressive responses and failure behaviors of composite graded auxetic re-entrant honeycomb structure. *Thin-Walled Struct.* **187**, 110721 (2023). <https://doi.org/10.1016/j.tws.2023.110721>
15. Wang, Y.: Auxetic composite laminates with through-thickness negative Poisson's ratio for mitigating low velocity impact damage: a numerical study. *Materials*. **15**, 6963 (2022). <https://doi.org/10.3390/ma15196963>
16. Jiang, L., Hu, H.: Finite element modeling of multilayer orthogonal auxetic composites under low-velocity impact. *Materials*. **10**, 908 (2017). <https://doi.org/10.3390/ma10080908>
17. Hou, S., Li, T., Jia, Z., Wang, L.: Mechanical properties of sandwich composites with 3d-printed auxetic and non-auxetic lattice cores under low velocity impact. *Mater. Des.* **160**, 1305–1321 (2018). <https://doi.org/10.1016/j.matdes.2018.11.002>
18. Novak, N., Vesenjok, M., Kennedy, G., Thadhani, N., Ren, Z.: Response of chiral auxetic composite sandwich panel to fragment simulating projectile impact. *Phys. status solidi*. **257**, 1900099 (2020). <https://doi.org/10.1002/pssb.201900099>
19. Usta, F., Türkmen, H.S., Scarpa, F.: Low-velocity impact resistance of composite sandwich panels with various types of auxetic and non-auxetic core structures. *Thin-Walled Struct.* **163**, 107738 (2021). <https://doi.org/10.1016/j.tws.2021.107738>
20. Tomita, S., Shimanuki, K., Oyama, S., Nishigaki, H., Nakagawa, T., Tsutsui, M., Emura, Y., Chino, M., Tanaka, H., Itou, Y., Umemoto, K.: Transition of deformation modes from bending to auxetic compression in origami-based metamaterials for head protection from impact. *Sci. Rep.* **13**, 12221 (2023). <https://doi.org/10.1038/s41598-023-39200-8>
21. Petit, A., Ayagara, A.R., Langlet, A., Delille, R., Parmantier, Y.: Influence of auxetic structure parameters on dynamic impact energy absorption. In: *Tiwari, R., Ram Mohan, Y.S., Darpe, A.K., Kumar, V.A., Tiwari, M. (eds.) Vibration Engineering and Technology of Machinery, Volume II. VETOMAC 2021, Mechanisms and Machine Science*, vol. 153, pp. 479–495 (2024). [https://doi.org/10.1007/978-981-99-8986-7\\_32](https://doi.org/10.1007/978-981-99-8986-7_32)
22. Biglari, H., Teymouri, H., Foroutan, M.: Application of auxetic core to improve dynamic response of sandwich panels under low-velocity impact. *Arab. J. Sci. Eng.* (2024). <https://doi.org/10.1007/s13369-024-08817-w>

23. Hoseinlghab, S., Farahani, M., Safarabadi, M., Nikkhah, M.: Tension-after-impact analysis and damage mechanism evaluation in laminated composites using AE monitoring. *Mech. Syst. Sig. Process.* **186**, 109844 (2023). <https://doi.org/10.1016/j.ymsp.2022.109844>
24. Hoseinlghab, S., Farahani, M., Safarabadi, M., Jalali, S.S.: Comparison and identification of efficient nanoparticles to improve the impact resistance of glass/epoxy laminates: experimental and numerical approaches. *Mech. Adv. Mater. Struct.* **30**, 694–709 (2023). <https://doi.org/10.1080/15376494.2021.2023914>
25. Hoseinlghab, S., Farahani, M., Safarabadi, M.: Improving the impact resistance of the multilayer composites using nanoparticles. *Mech. Based Des. Struct. Mach.* **51**, 3083–3099 (2023). <https://doi.org/10.1080/15397734.2021.1917424>
26. Alderson, K.L., Coenen, V.L.: The low velocity impact response of auxetic carbon fibre laminates. *Phys. status solidi.* **245**, 489–496 (2008). <https://doi.org/10.1002/pssb.200777701>
27. Brańka, A.C., Heyes, D.M., Wojciechowski, K.W.: Auxeticity of cubic materials. *Phys. status solidi.* **246**, 2063–2071 (2009). <https://doi.org/10.1002/pssb.200982037>
28. Tsai, S.W., Hahn, H.T.: Introduction to composite materials. Technomic Publ. Co., Westport (1980)
29. Fan, Y., Wang, Y.: The effect of negative Poisson's ratio on the low-velocity impact response of an auxetic nanocomposite laminate beam. *Int. J. Mech. Mater. Des.* **17**, 153–169 (2021). <https://doi.org/10.1007/s10999-020-09521-x>
30. Donoghue, J.P.: Negative Poisson's ratio effects on the mechanical performance of composite laminates. University of Liverpool, Liverpool (1995)
31. Evans, K.E., Donoghue, J.P., Alderson, K.L.: The design, matching and manufacture of auxetic carbon fibre laminates. *J. Compos. Mater.* **38**, 95–106 (2004). <https://doi.org/10.1177/0021998304038645>
32. Herakovich, C.T.: Composite laminates with negative through-the-thickness Poisson's ratios. *J. Compos. Mater.* **18**, 447–455 (1984). <https://doi.org/10.1177/002199838401800504>
33. Hadi Harkati, E.L., Bezazi, A., Scarpa, F., Alderson, K., Alderson, A.: Modelling the influence of the orientation and fibre reinforcement on the Negative Poisson's ratio in composite laminates. *Phys. status solidi.* **244**, 883–892 (2007). <https://doi.org/10.1002/pssb.200572707>
34. Coenen, V.L., Alderson, K.L.: Mechanisms of failure in the static indentation resistance of auxetic carbon fibre laminates. *Phys. status solidi.* **248**, 66–72 (2011). <https://doi.org/10.1002/pssb.201083977>
35. Paris, F., Jackson, K.E.: A study of failure criteria of fibrous composite materials. No. NAS 1.26: 210661, 2001
36. Lee, C.S., Kim, J.H., Kim, S.K., Ryu, D.M., Lee, J.M.: Initial and progressive failure analyses for composite laminates using Puck failure criterion and damage-coupled finite element method. *Compos. Struct.* **121**, 406–419 (2015). <https://doi.org/10.1016/j.compstruct.2014.11.011>
37. Liu, P.F., Liao, B.B., Jia, L.Y., Peng, X.Q.: Finite element analysis of dynamic progressive failure of carbon fiber composite laminates under low velocity impact. *Compos. Struct.* **149**, 408–422 (2016). <https://doi.org/10.1016/j.compstruct.2016.04.012>
38. Li, X., Ma, D., Liu, H., Tan, W., Gong, X., Zhang, C., Li, Y.: Assessment of failure criteria and damage evolution methods for composite laminates under low-velocity impact. *Compos. Struct.* **207**, 727–739 (2019). <https://doi.org/10.1016/j.compstruct.2018.09.093>
39. Sokolinsky, V.S., Indermuehle, K.C., Hurtado, J.A.: Numerical simulation of the crushing process of a corrugated composite plate. *Compos. Part A Appl. Sci. Manuf.* **42**, 1119–1126 (2011). <https://doi.org/10.1016/j.compositesa.2011.04.017>
40. Benzeggagh, M.L., Kenane, M.J.: Measurement of mixed-mode delamination fracture toughness of unidirectional glass/epoxy composites with mixed-mode bending apparatus. *Compos. Sci. Technol.* **56**, 439–449 (1996). [https://doi.org/10.1016/0266-3538\(96\)00005-X](https://doi.org/10.1016/0266-3538(96)00005-X)
41. Alderson, K.L., Simkins, V.R., Coenen, V.L., Davies, P.J., Alderson, A., Evans, K.E.: How to make auxetic fibre reinforced composites. *Phys. status solidi.* **242**, 509–518 (2005). <https://doi.org/10.1002/pssb.200460371>
42. Hongkarnjanakul, N., Bouvet, C., Rivallant, S.: Validation of low velocity impact modelling on different stacking sequences of CFRP laminates and influence of fibre failure. *Compos. Struct.* **106**, 549–559 (2013). <https://doi.org/10.1016/j.compstruct.2013.07.008>

**Publisher's Note** Springer Nature remains neutral with regard to jurisdictional claims in published maps and institutional affiliations.

Springer Nature or its licensor (e.g. a society or other partner) holds exclusive rights to this article under a publishing agreement with the author(s) or other rightsholder(s); author self-archiving of the accepted manuscript version of this article is solely governed by the terms of such publishing agreement and applicable law.